Synthesis, Structure Determination from Powder Diffraction Data, and Thermal Behavior of Lead Zirconium Oxalate Hydrate $Pb_2Zr(C_2O_4)_4 \cdot nH_2O$ ($3 < n < 9$)

C. Boudaren,[†] J. P. Auffrédic, M. Louër, and D. Louër*,[‡]

Laboratoire de Chimie du Solide et Inorganique Moléculaire (UMR CNRS 6511), Groupe de Cristallographie des Poudres et Réactivité des Solides, Université de Rennes 1, Avenue du Général Leclerc, 35042 Rennes Cedex, France

Received April 12, 2000. Revised Manuscript Received May 19, 2000

A new mixed lead zirconium oxalate, $Pb_2Zr(C_2O_4)_4 \cdot nH_2O$ ($3 < n < 9$), has been prepared from precipitation of a nitric solution of lead and zirconium cations by an oxalic solution at 345 K. The crystal structure of $Pb_2Zr(C_2O_4)_4 \cdot 6H_2O$ has been determined ab initio from powder diffraction data collected with conventional monochromatic X-rays. The symmetry is monoclinic, space group *C*2/*c* (No. 15), cell dimensions $a = 9.537(1)$ Å, $b = 29.622(3)$ Å, $c = 8.9398(9)$ Å, $\beta = 121.19(4)°$, and $Z = 4$. The complex three-dimensional structure is built from 8-fold-coordinated zirconium atoms and 9-fold- and 8-fold-coordinated lead atoms linked by oxalate groups. Only one water molecule has been found free in the structure. The dehydration is reversible, and the cell parameters vary between the composition limits without a major change of the crystal structure framework. A thermodynamical study has demonstrated the zeolitic nature of the water molecules. The enthalpy, $\Delta_r H$, and entropy, $\Delta_r S$, of the dehydration reaction have been determined as a function of the number of zeolitic water molecules. The complete decomposition scheme of the anhydrous phase $Pb_2Zr(C_2O_4)_4$ into $PbZrO_3$ and finally ZrO_2, studied from temperature-dependent X-ray powder diffraction and thermogravimetric analysis, is carefully described.

1. Introduction

There is a considerable technological interest in ferroelectric PZT type materials for their ability to switch their polarization direction between two stable polarized states. Indeed, PZT ceramics are potential candidates for nonvolatile ferroelectric random-access memories[1] and they are used for other various electronic applications resulting from their piezoelectric and pyroelectric properties. Lead zirconate titanate $PbZr_xTi_{1-x}O_3$ (PZT), is a binary solid solution system between lead titanate $PbTiO_3$ (PT) and lead zirconate $PbZrO_3$ (PZ). PZT powders are generally prepared using different methods, such as solid-state reactions of the constituent metal oxides and carbonates, from which compositional inhomogeneities are often observed, and non-oxide routes as hydroxide coprecipitation or dried alkoxide-based gels. Another method is from the thermal decomposition of mixed precursors with low thermal stability. A representative example is the formation of pure $BaTiO_3$ from barium titanyl oxalate hydrate.[2] In the PZT family, the preparation of PZ and PT from the pyrolysis of lead zirconyl oxalate and lead titanyl oxalate precursors have been reported.[3,4] However, very little structural information about the precursors is known and the elucidation of the decomposition processes was usually based essentially on thermogravimetric measurements. Then, there is an interest in investigating carefully the chemistry and crystal chemistry of the precursors of such mixed oxides. In this way the noteworthy recent advances in powder diffraction offer new tools to investigate both the crystal structure and the thermal behavior of these kinds of materials often obtained in a powder form.[5,6] The present study deals with the preparation of a new mixed lead and zirconium oxalate compound with a complex crystal structure determined ab initio from powder diffraction data collected with a conventional X-ray source. In addition, the stoichiometry in water molecule content is thoroughly investigated, as well as the thermal behavior of this material studied by means of temperature-dependent powder diffraction and conventional thermal analysis.

2. Experimental Section

2.1. Material Preparation. The precipitate $Pb_2Zr(C_2O_4)_4 \cdot nH_2O$ was obtained by titration of a nitric solution of lead and

[†] Permanent address: Institut de Chimie, Université de Constantine, 25000 Constantine, Algeria.

[‡] E-mail address: Daniel.Louër@univ-rennes1.fr. Tel. no.: (33) 2 99 28 62 48. Fax no.: (33) 2 99 38 34 87.

(1) Auciello, O.; Scott, J. F.; Ramesh, R. *Phys. Today* **1998**, *51*, 22−27.

(2) Louër, M.; Louër, D.; Gotor, F. J.; Criado, J. M. *J. Solid State Chem.* **1991**, *92*, 565−572.

(3) Sharma, A. K.; Kaushik, N. K. *Thermochim. Acta* **1985**, *83*, 347−376.

(4) Sekar, M. A.; Dhanaraj, G.; Bhat, H. L.; Patil, K. C. *J. Mater. Sci.* **1992**, *3*, 237−239.

(5) Langford, J. I.; Louër, D. *Rep. Prog. Phys.* **1996**, *59*, 131−234.

(6) Louër, D. *Acta Crystallogr.* **1998**, *A54*, 922−933.

10.1021/cm001063j CCC: $19.00 © 2000 American Chemical Society
Published on Web 07/26/2000

zirconium cations by an oxalic acid solution. The conditions to obtain a pure compound were as follows: 1 g of zirconium dinitrate oxide $ZrO(NO_3)_2$ from Alpha (purity 99.9%) [whose correct chemical formula is in fact $Zr(OH)_2(NO_3)_2 \cdot (1 + x)H_2O$[7]] and 0.62 g of lead nitrate $Pb(NO_3)_2$ (Prolabo, rectapur) were dissolved at room temperature in 200 mL of 3 mol L^{-1} nitric acid solution. This solution was heated at 345 K and slowly titrated under constant stirring by a 0.5 mol L^{-1} oxalic acid solution in excess to ensure the complete precipitation. The white precipitate was filtered off, washed with distilled water, and dried at room temperature. The chemical formula was confirmed from thermogravimetric analysis, manganimetric titration of the oxalate content (experimental: 35.06%), energy dispersive spectrometry (ratio Pb/Zr: 1.92), and the determination of the crystal structure of $Pb_2Zr(C_2O_4)_4 \cdot 6H_2O$ described in the present study. As shown from this study the content in water molecules (n) depends on the partial water vapor pressure in the ambient atmosphere. It was found 8.5 when the pressure is 13 Torr.

2.2. Collection of High-Resolution Powder X-ray Diffraction Data. High-quality X-ray powder diffraction data were obtained for a compound with the structural formula $Pb_2Zr(C_2O_4)_4 \cdot 6H_2O$ with a Siemens D500 diffractometer using a pure monochromatic Cu Kα_1 radiation (λ = 1.5406 Å) as described elsewhere.[8] To reduce preferred orientation effects the powder was mounted in a top-loaded sample holder.[9] The diffraction pattern was recorded under ambient atmosphere over the angular range 5−110° (2θ), with a step length of 0.02° (2θ) and a counting time of 27.5 s step^{-1} until 60° (2θ) and 55 s step^{-1} from 60.02° (2θ) to the end of the scan. Then, the full pattern was scaled to 27.5 s step^{-1}. After data collection, the stability of the X-ray source was checked by recording again the diffraction lines at low angles. A correction of intensities collected at angles below 20° (2θ) was applied from the changes in integrated intensities obtained for data collected with a narrower receiving slit.

Diffraction data were also collected at room temperature with the Siemens D500 diffractometer under various water vapor pressures from a sample located in a tight sample holder. Partial water vapor pressures $P'(H_2O)$ were generated by bubbling nitrogen at a flow rate of 40 mL min^{-1} in sulfuric acid solutions with a known concentration and kept at selected temperatures. The water vapor pressure range covered was 0.2−15 Torr. Moreover, additional diffraction data were collected in situ at various temperatures with a Bruker D5005 diffractometer, using Cu Kα radiation [λ(Kα_1) = 1.5406 Å, λ(Kα_2) = 1.5444 Å] selected with a diffracted-beam monochromator, equipped with a Anton Paar HTK1200 high-temperature oven camera.

The extraction of peak positions for indexing was performed with the Socabim fitting program PROFILE, available in the PC software package DIFFRAC-AT supplied by Bruker AXS. Pattern indexing was carried out by means of the program DICVOL91.[10] The program EXPO[11] was used for structure solution, and Rietveld refinements were performed with FULLPROF99,[12] available in the software package WINPLOTR.[13] The software DIAMOND (version 2.1) was used for structure drawings.

2.3. Thermal Analyses. Temperature-dependent X-ray diffraction (TDXD) was performed with a powder diffractometer combining the curved-position-sensitive detector (PSD) from INEL (CPS 120) and a high-temperature attachment from Rigaku. The detector was used in a semifocusing arrangement by reflection (Cu Kα_1 radiation) as described elsewhere.[14] With this geometry the flat sample is stationary. An angle of 6° between the incident beam and the surface of the sample was selected. The thermal decomposition of $Pb_2Zr(C_2O_4)_4 \cdot nH_2O$ was carried out under nitrogen, under vacuum, and under selected water vapor pressures.

Thermogravimetric analyses (TG) were carried out either with a Rigaku Thermoflex instrument or a MacBain type thermobalance. With the first instrument, the runs were performed under a partial water vapor pressure $P'(H_2O)$ generated in the same manner as described above. With the second one, the experiments were conducted under vacuum or a total water vapor pressure $P(H_2O)$ in the range 0.05−20 Torr. To generate this water vapor pressure the thermobalance connected to a bulb containing a sulfuric acid solution was evacuated until the sulfuric solution boiled and was then isolated from the vacuum pump. Different values of $P(H_2O)$ were obtained by changing the concentration and the temperature of the sulfuric solution. The values of $P(H_2O)$ were calculated from tables edited by Boll.[15] The powdered samples were spread evenly in large platinum crucibles to avoid mass effects.

Table 1. Crystallographic Data and Details of the Rietveld Refinement for $Pb_2Zr(C_2O_4)_4 \cdot 6H_2O$

cryst system and space group	monoclinic *C*2/*c*
Z	4
a (Å)	9.537(1)
b (Å)	29.622(3)
c (Å)	8.9398(9)
β (deg)	121.19(4)
V (Å^3)	2160.5(3)
wavelength (Å)	1.5406
2θ range (deg)	5−110
step scan increment (deg in 2θ)	0.02
no. of reflcns	1369
no. of refined params (including 8 B params; see Table 2)	79
no. of atoms	19
R_F	0.051
R_B	0.101
R_P	0.131
R_{WP}	0.173

3. Ab Initio Structure Determination of $Pb_2Zr(C_2O_4)_4 \cdot 6H_2O$

3.1. Pattern Indexing. The first 20 lines of the X-ray powder diffraction pattern, with an absolute error of 0.02° (2θ) on peak positions, were indexed on the basis of a monoclinic solution with high figures of merit (for definitions see ref 5), i.e., M_{20} = 43 and F_{20} = 104(0.0033,58). The unit cell parameters are given in Table 1. From the analysis of the powder data available the systematic absences were found consistent with the space groups *Cc* and *C*2/*c*. The centrosymmetric space group *C*2/*c* was subsequently found to be correct from the structure determination. The powder data have been submitted to the ICDD[16] for possible inclusion in the Powder Data File. The indexing solution was used to interrogate the NIST-CDF database[16] from which no chemically related isostructural material was found. Despite the quite large unit cell (2160.5 Å^3) the powder diffraction data were used to solve the crystal structure.

(7) Bénard-Rocherullé, P.; Rius, J.; Louër, D. *J. Solid State Chem.* **1997**, *128*, 295−304.
(8) Louër, D.; Langford, J. I. *J. Appl. Crystallogr.* **1988**, *21*, 430−437.
(9) Swanson, H. E.; Morris M. C.; Evans, E. H.; Ulmer, L. *Natl. Bur. Stand.* (*U.S.*) **1964**, *Monogr. 25*, 3, 1−3.
(10) Boultif, A.; Louër, D. *J. Appl. Crystallogr.* **1991**, *24*, 987−993.
(11) Altomare, A.; Burla, M. C.; Camalli, M.; Carrozzini, G. L.; Cascarano, G.; Giacovazzo, C.; Guagliardi, A.; Moliterni, A. G. G.; Polidori, G.; Rizzi, R. *J. Appl. Crystallogr.* **1999**, *32*, 339−340.
(12) Rodriguez-Carvajal, J. In *Collected Abstracts of Powder Diffraction Meeting*; Toulouse, France, 1990; pp 127−128.
(13) Rodriguez-Carvajal, J.; Roisnel, T. *IUCr Comm. Powder Diffract. Newslett.* **1998**, *20*, 35.
(14) Plévert, J.; Auffrédic, J. P.; Louër, M.; Louër, D. *J. Mater. Sci.* **1989**, *24*, 1913−1918.
(15) Boll, M. *Mémento du Chimiste* (Memento for Chemists); Dunod: Paris, 1949.
(16) International Centre for Diffraction Data, PDF Database, Newtown Square, PA.

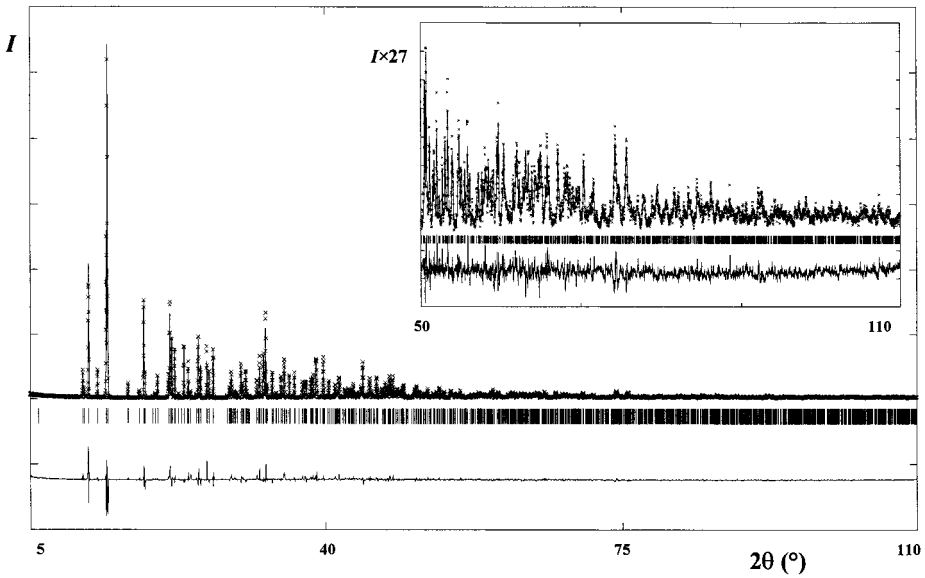

Figure 1. Final Rietveld refinement plot for $Pb_2Zr(C_2O_4)_4 \cdot 6H_2O$. The experimental data are represented by crosses, while the calculated pattern is shown by the solid line. The lower trace is the difference curve between observed and calculated patterns. The Bragg reflections are shown by the vertical bars.

3.2. Structure Determination. Integrated intensities were extracted from the pattern decomposition iterative algorithm available in EXPO and subsequently used to solve the structure by the direct methods. The range 10−70° (2θ) offered a reasonable compromise between the number of reflections (478) and the number of statistically independent reflections (37%), according to the degree of diffraction line overlap.[17] The first three maxima in the *E*-map with the highest figure of merit were assigned to two Pb and one Zr atoms located on the 2-fold axis. No additional light atom could be identified with certainty. The remaining part of the structure was found from several somewhat laborious difference Fourier calculations with the program SHELXL-97.[18] The approximate solution was used as starting structural model for a Rietveld refinement based on the whole angular range 5−110° (2θ). A pseudo-Voigt function was selected to describe individual line profiles, and the usual quadratic function in tan θ was used to describe the angular dependence of peak widths. The background was described with a polynomia of degree 5. The distances within the oxalate groups were restrained to 1.25(5) Å for C−O and 1.55(5) Å for C−C to keep them in a reasonable conformation. At the end of the refinement, a last difference Fourier map calculation showed a peak, nonbonded to the cations, which was ascribed to a water molecule (Ow4). At this stage of the study the chemical formula of the sample investigated was $Pb_2Zr(C_2O_4)_2 \cdot 6H_2O$. It should be noted that an additional refinement from a second diffraction data set collected for a sample under nitrogen did not reveal this last water molecule. On the other hand, no remaining atom could be detected from a final Fourier map, which means that from the crystallographic study only 6 water molecules have been localized from the diffraction data collected in air. The details of the Rietveld refinement are given in Table 1. Figure 1 shows the final fit between observed and calculated patterns. Final atomic parameters are given in Table 2, and selected distances and angles, in Table 3.

Table 2. Fractional Atomic Coordinates and Displacement Parameters[a] for $Pb_2Zr(C_2O_4)_4 \cdot 6H_2O$

atom	*x*	*y*	*z*	*B* (Å^2)
Pb1	0.5	0.0264(1)	0.25	1.10(8)
Pb2	0.0	0.2605(1)	0.25	1.10(8)
Zr	0.0	0.1162(2)	0.75	0.5(2)
C1	−0.104(2)	0.186(1)	0.918(3)	0.2(6)
C2	0.079(2)	0.177(1)	1.060(2)	0.2(6)
O1	−0.181(2)	0.2173(7)	0.942(5)	1.6(3)
O2	−0.163(3)	0.1634(7)	0.779(2)	1.6(3)
O3	0.137(3)	0.1488(8)	1.001(3)	1.6(3)
O4	0.158(3)	0.1932(9)	1.212(2)	1.6(3)
C3	0.180(2)	0.054(1)	0.628(1)	0.2(6)
C4	0.287(2)	0.057(1)	0.831(1)	0.2(6)
O5	0.053(2)	0.0774(8)	0.564(2)	1.6(3)
O6	0.238(3)	0.0365(8)	0.543(3)	1.6(3)
O7	0.429(2)	0.0404(9)	0.914(3)	1.6(3)
O8	0.220(2)	0.0787(8)	0.898(3)	1.6(3)
Ow1	0.5	0.116(2)	0.25	6(1)
Ow2	0.023(6)	0.311(1)	−0.013(6)	9(1)
Ow3	0.228(4)	0.0535(8)	0.263(4)	1.0(9)
Ow4	0.5	−0.241(2)	0.75	10(1)

[a] The atomic displacement parameters of O atoms and C atoms were allowed to vary in the same manner.

3.3. Description of the Structure. The complex three-dimensional structure of $Pb_2Zr(C_2O_4)_4 \cdot 6H_2O$ is built from zirconium and lead polyhedra linked by oxalate groups. The Zr atom is 8-fold coordinated by O atoms from bidentate oxalate groups. The Zr coordination polyhedra can be described as a distorted square antiprism with distances Zr−O in the range 2.12−2.28 Å (Figure 2a). The deviation from the mean plane of atoms O2(×2) and O3(×2) is 0.23 Å. The other basis [O5(×2) and O8(×2)] is almost perfect since the maximum deviation from planarity is 0.008 Å. The deviation from ideal square bases can be seen from Table 3. These two planes are parallel and are rotated according an angle of about 45°. The distances of Zr atom from the

(17) Altomare, A.; Cascarano, G.; Giacovazzo, C.; Guagliardi, A.; Moliterni, A. G. G.; Burla, M. C.; Polidori, G. *J. Appl. Crystallogr.* **1995**, *28*, 738−744.

(18) Sheldrick, G. M. SHELXL-97, Program for Crystal Structure Refinement, University of Göttingen, Göttingen, Germany, 1997.

Table 3. Selected Bond Distances (Å) and Angles (deg) with Their Standard Deviations for $Pb_2Zr(C_2O_4)_4{\cdot}6H_2O$[a]

metal coordination		bases of the antiprism	
		Pb1	
Pb1−O6$^{I, II}$	2.89(2)	O7^{I}−O6^{I}	2.84(3)
Pb1−O7$^{III, IV}$	2.75(2)	O7^{I}−O6^{II}	3.00(4)
Pb1−O7$^{I, II}$	2.75(2)	O7^{III}−Ow3	4.44(4)
Pb1−Ow1	2.66(5)	O7^{III}−Ow3^{IV}	3.07(5)
Pb1−Ow3, Ow3^{V}	2.77(4)	O6^{I}−O7^{I}−O6^{II}	98(1)
		O7^{I}−O6^{I}−O6^{II}	82(1)
		Ow3−O7^{III}−Ow3^{V}	88(2)
		O7^{II}−Ow3−O7^{IV}	91(1)
		Pb2	
Pb2−O1$^{III, VI}$	2.70(2)	O1^{II}−O4^{III}	2.95(3)
Pb2−O1$^{VII, VIII}$	2.69(3)	O1^{III}−O4^{VI}	3.17(3)
Pb2−O4$^{III, VI}$	2.62(3)	O1^{VII}−Ow2	3.65(4)
Pb2−Ow2, Ow2^{IX}	2.90(5)	O1^{VII}−Ow2^{IX}	3.73(7)
		O4^{III}−O1^{III}−O4^{VI}	73(1)
		O1^{III}−O4^{III}−O1^{VI}	104(1)
		Ow2−O1^{VII}−Ow2^{IX}	84(2)
		O1^{VII}−Ow2−O1^{VIII}	90(1)
		Zr	
Zr−O2, O2^{VI}	2.20(3)	O2−O3	2.54(3)
Zr−O3, O3^{VI}	2.15(2)	O2−O3^{VI}	2.67(5)
Zr−O5, O5^{VI}	2.28(2)	O5−O8	2.56(3)
Zr−O8, O8^{VI}	2.12(2)	O5−O8^{VI}	2.79(3)
		O2−O3−O2^{VI}	95(1)
		O2−O3−O2^{VI}	81(1)
		O5−O8−O5^{VI}	95(1)
		O8−O5−O8^{VI}	85(2)
		Possible H-bonds	
Ow1−Ow2$^{X, XI}$	2.94(6)	Ow2^{X}−Ow1−Ow2^{XI}	87(2)
Ow2−O2^{VII}	2.86(5)	O2^{VII}−Ow2−Ow4^{XIII}	121(1)
Ow2−Ow1^{XII}	2.94(6)	O2^{VII}−Ow2−Ow1^{XII}	97(2)
Ow2−Ow4^{XIII}	2.54(4)	Ow1^{XII}−Ow2−Ow4^{XIII}	84(2)
Ow3−O5^{IX}	2.85(4)	O5^{IX}−Ow3−O6	127(1)
Ow3−O6	2.50(4)		

[a] Symmetry code: **I**, $x, -y, z - 0.5$; **II**, $1 - x, -y, 1 - z$; **III**, $x, y, z - 1$; **IV**, $1 - x, y, 1.5 - z$; **V**, $1 - x, y, 0.5 - z$; **VI**, $-x, y, 1.5 - z$; **VII**, $0.5 + x, 0.5 - y, z - 0.5$; **VIII**, $-x - 0.5, 0.5 - y, 1 - z$; **IX**, $-x, y, 0.5 - z$; **X**, $0.5 + x, 0.5 - y, 0.5 + z$; **XI**, $0.5 - x, 0.5 - y, -z$; **XII**, $x - 0.5, 0.5 - y, z - 1$; **XIII**, $x - 0.5, 0.5 + y, z - 1$.

two planes are 1.20 and 1.15 Å. There are two lead atoms in the asymmetric unit. Pb1 is 9-fold coordinated in the form of a highly distorted square antiprism monocapped by a water molecule Ow1 (Figure 2b). It is surrounded by 6 O atoms from two bidentate oxalate groups (O6^{I}, O7^{I} and O6^{II}, O7^{II}) and two monodentate oxalate groups (O7^{III} and O7^{IV}). The distances Pb1−O are in the range 2.75−2.89 Å. In addition there are three water molecules linked to Pb1 at 2.66 and 2.77 Å (×2). One of the square bases is formed by four bidentate oxalate oxygen atoms. The deviation from the mean plane is 0.06 Å. The other base is formed by two monodentate oxalate oxygen atoms and two water molecules. The deviation from the mean plane is 0.22 Å. The mean planes of the polyhedra are parallel since Pb1 is located on a binary axis. The distance of the lead atom to the plane capped by Ow1 is shorter (0.58 Å) with respect to its distance to the opposite square face (1.84 Å). The second lead atom Pb2 is 8-fold coordinated (Figure 2c) with six O atoms belonging to two bidentate and two monodentate oxalate groups (distances ranged from 2.62 to 2.70 Å) and two water molecules at 2.90 Å. The polyhedron can be described as highly distorted square antiprism. The deviations from the mean planes are 0.31 Å for the oxalate-oxygen-based face and 0.28 Å for the second face in which water molecules are

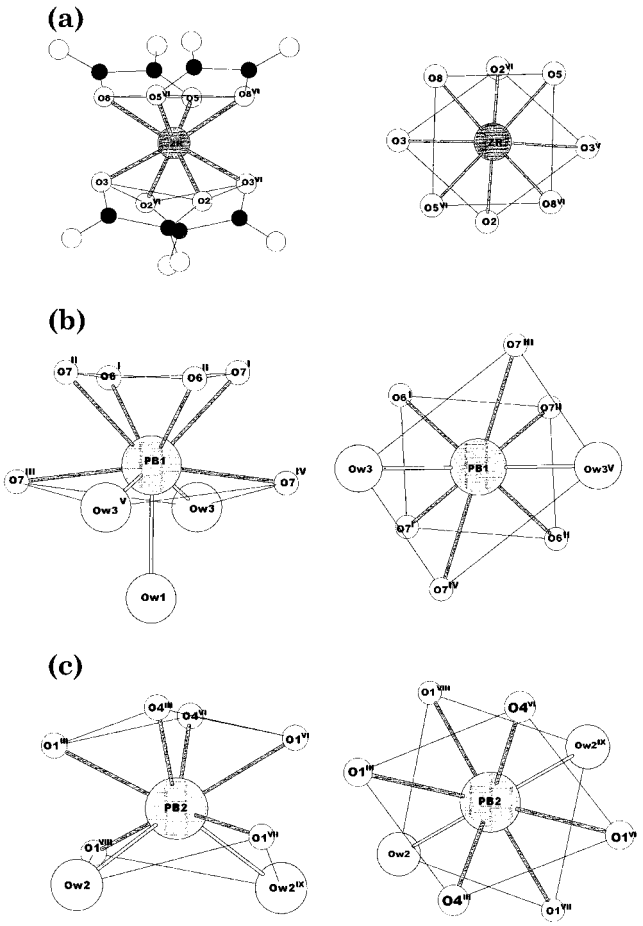

Figure 2. Coordination polyhedra of (a) Zr, (b) Pb1, and (c) Pb2 atoms.

involved. Pb2 is closer to the plane containing the water molecules (0.98 Å vs 1.60 Å to the second face). The mean planes also are parallel. The distortion of the square bases can be seen in Table 3.

Figure 3 is a projection of the structure along [001]. It shows how the metal atoms alternate, i.e., Pb1 ($y = \pm 0.026$), Zr ($y = 0.116$), Pb2 ($y = 0.26$), and Zr ($y = 0.384$). This sequence continues at $^1/_2 + y$ due to the *C* lattice. Figure 4 shows partial projections on the plane (*a*,*c*), i.e., the condensation of edge-sharing Pb1−O9 polyhedra to form chains along [001] (Figure 4a), the isolated Zr ($y = 0.116$) polyhedra (Figure 4b), and the condensation of edge-sharing Pb2−O8 polyhedra to form chains along [101] (Figure 4c). The connection between these structural fragments is carried out by the oxalate groups to form the three-dimensional network (Figure 3). There are two independent oxalate groups: ox1 (C1, C2, O1−4); ox2 (C3, C4, O5−8). The oxalate group ox1 acts as a bidentate ligand with the neighboring Zr and Pb2 coordination polyhedra and is also linked to another Pb2 atom by one O atom. It ensures the connection between the planes located at $y = 0.116$ and $y = 0.26$. The oxalate group ox2 acts as a bidentate ligand with the neighboring Zr and Pb1 coordination polyhedra and is also linked by one O atom to another Pb1 atom. It ensures the connection between planes at $y = \pm 0.026$ and $y = 0.116$.

The water molecules Ow1 and Ow3 are linked to Pb1, and Ow2 is linked to Pb2. The free water molecule (Ow4) is not shown on the projection in Figure 3,

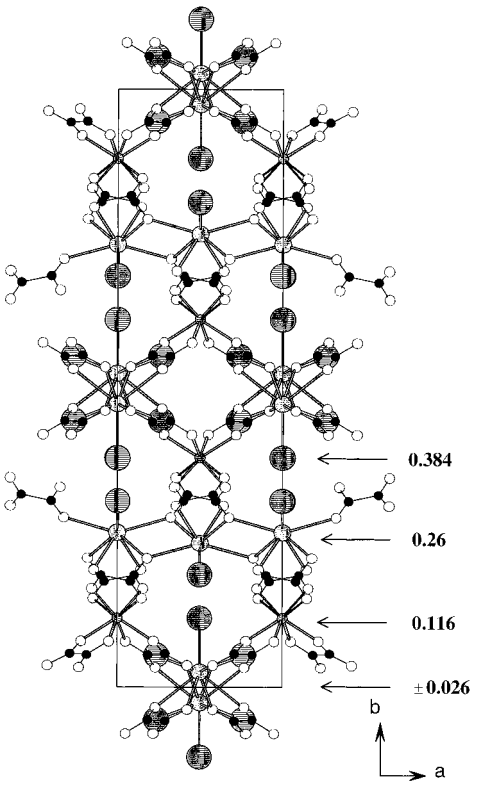

Figure 3. Projection of the structure of $Pb_2Zr(C_2O_4)_4 \cdot 6H_2O$ along the *c* axis: large dark-gray circle, H_2O; medium light-gray circle, Pb; small light-gray circle, Zr.

because it is superposed to Pb2. As already mentioned, this molecule was only detected at the last difference Fourier calculation. It is worth noting the high value of its isotropic displacement parameter, 10(1) Å^2, as well as those of two other water molecules, Ow1 and Ow2, with the displacement parameters 6(1) Å^2 and 9(1) Å^2 (Table 2). Although the atomic displacement parameters of light atoms are usually not reliable with X-ray powder diffraction data (small values and even negative values are often calculated due to high correlations with the background level), the high values observed here for the free water molecule, as well as for two bonded molecules, must be indicative of a high motion. This result is consistent with the fact that the free water molecule Ow4 could not be detected in the structure refinement of a second data set obtained from a sample preserved under nitrogen atmosphere during data collection and also with the thermodynamical study reported below showing the zeolitic properties of the water molecules.

3.4. Influence of the Water Content on the Cell Parameters. The water content *n* in the sample being investigated has been found to be 6 from the structure determination. However, as it has just been noted the magnitude of certain atomic displacement parameters for water-molecule oxygen is likely associated to water vapor pressure dependent properties. This feature has been evidenced by additional experiments carried out from TG measurements. This is shown in Figure 5 with the changes of *n*, at 22 °C, with either the total pressure $P(H_2O)$ or the partial pressure $P'(H_2O)$. It can be seen that the hydration rate of the precursor is greater when it is submitted to $P'(H_2O)$, e.g., 7.2 for $P(H_2O) = 15$ Torr and 9.2 for $P'(H_2O) = 15$ Torr. The water content *n*

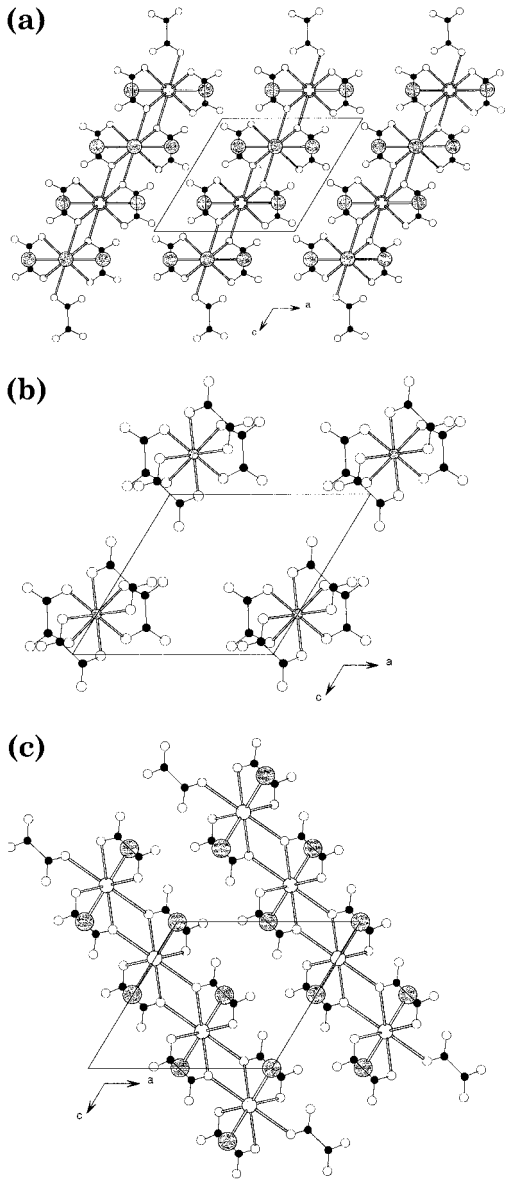

Figure 4. Partial views of the structure along the *b* axis: (a) $y = \pm 0.026$; (b) $y = 0.116$; (c) $y = 0.26$.

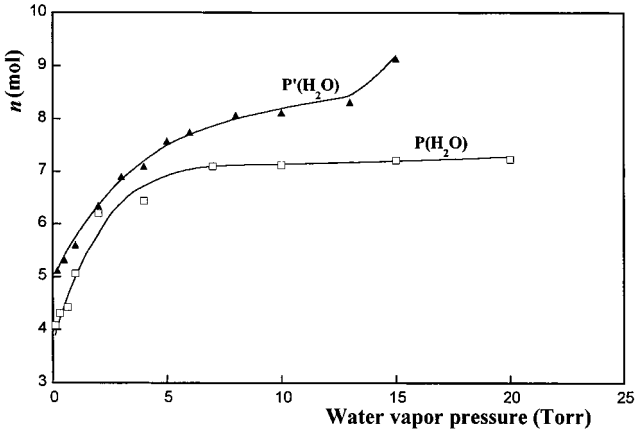

Figure 5. Water content *n* as a function of total $P(H_2O)$ or partial $P'(H_2O)$ water vapor pressure.

varies rapidly from ~4 to 7 for $P(H_2O)$ in the range 0.065−6 Torr and then slowly for higher pressures. On the contrary, it increases continuously with increasing

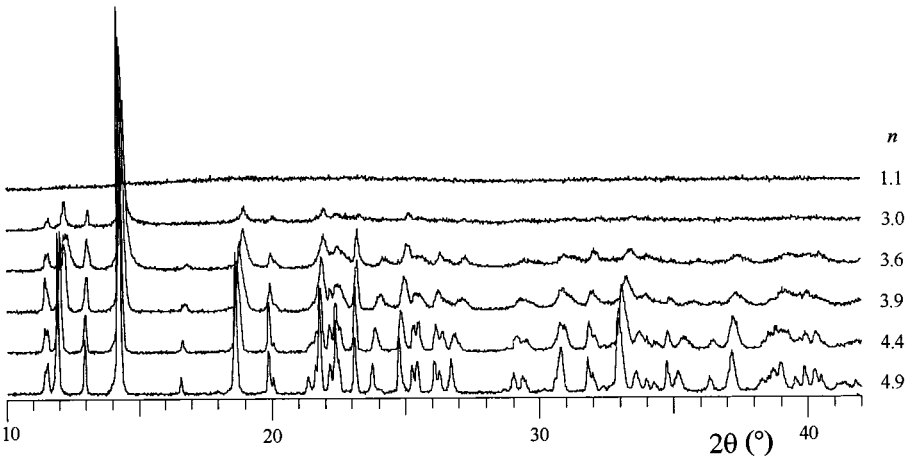

Figure 6. X-ray powder diffraction patterns of $Pb_2Zr(C_2O_4)_4 \cdot nH_2O$ ($n < 5$) as a function of the water content n.

$P'(H_2O)$ and is greater than 10 for pressures beyond 16 Torr without apparent deliquescence of the sample.

Nine X-ray powder diffraction patterns were collected at 22 °C from a sample located in a tight sample holder and subjected to various partial pressures $P'(H_2O)$ in the range 0.2−13 Torr; i.e., the water content in the sample changes from 5.1 to 8.5 H_2O molecules. The first 20 lines of the X-ray diffraction pattern obtained at 0.2 Torr ($n = 5.1$) were perfectly indexed on the basis of a monoclinic solution with high figures of merit. A least-squares refinement of the cell parameters from the resolved diffraction lines available gave the cell dimensions $a = 9.355(2)$ Å, $b = 29.715(5)$ Å, $c = 8.959(1)$ Å, $\beta = 120.95(1)°$, and $V = 2135.9(4)$ Å^3 [$M_{20} = 35$ and $F_{30} = 80(0.0094,40)$]. The cell parameters for the other eight diffraction patterns were refined using this solution as starting values. Additional diffraction patterns were also collected independently in situ from a sample located in the oven of the Bruker D5005 diffractometer under the water vapor pressure $P(H_2O) = 0.20$ Torr and submitted to temperatures selected to obtain a water content between 4.9 and 1.1 H_2O. However, as shown in Figure 6 the quality of the diffraction patterns deteriorates progressively as the sample loses water molecules until to be amorphous to X-rays. Pattern indexing and least-squares refinement of unit cell dimensions were conducted from available diffraction lines in the first four patterns according to the method described above.

Figure 7 shows the changes of the linear cell parameters and cell volume as a function of n. (The esd's values were in the ranges 0.001−0.002 Å for a and c, 0.003−0.006 Å for b, and 0.3−0.5° for β.) It can be seen that the unit cell volume decreases continuously during dehydration. It is the consequence of different behaviors of the cell parameters: c is nearly constant, a has a variation with an inflection point, b shows a maximum for n close to 5, and the angular parameter β is almost constant over the range 3.6−8.5 H_2O (mean value 121.5°). Somewhat related unit cell dimensions behaviors were reported recently when studying the zeolitic properties of $YK(C_2O_4)_2 \cdot 4H_2O$.[19] However, while in the last case the cell dimension changes with the water content were clearly understood from water molecules

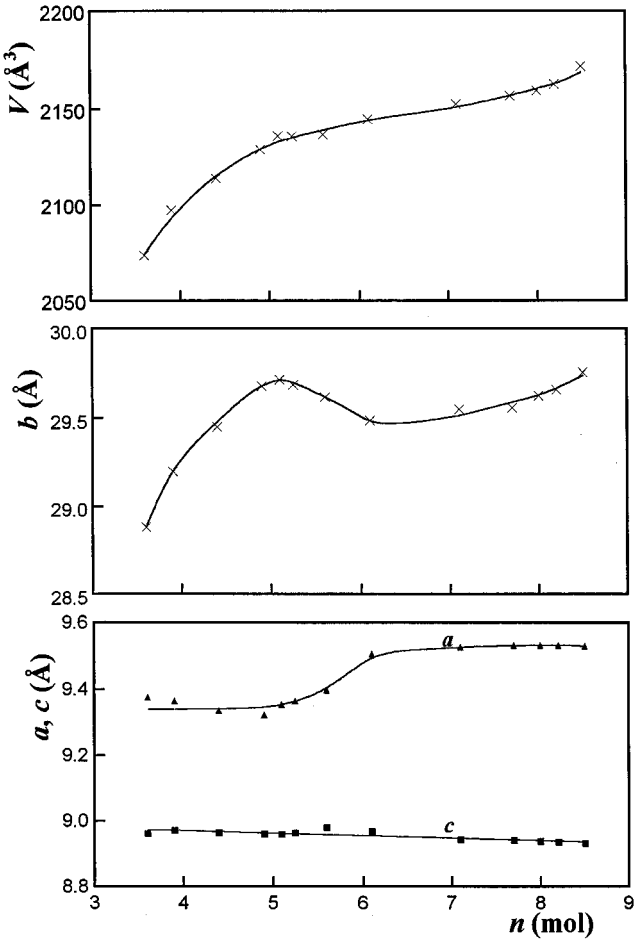

Figure 7. Behavior of the volume and linear parameters of the unit cell of $Pb_2Zr(C_2O_4)_4 \cdot nH_2O$ as a function of the number n of water molecules.

located in tunnels with square cross sections, the situation for the mixed Pb and Zr oxalate is more complicated since only one free water molecule (Ow4) has been detected in $Pb_2Zr(C_2O_4)_2 \cdot 6H_2O$. The release of this water molecule can explain the existence of hydrates in the range 5−6 H_2O without serious structure modification, except the decrease of the unit cell volume. Below 5 water molecules, the crystal symmetry is preserved; a lowering in the coordination number of the lead atoms must then be evoked to explain the departure of water molecules.

(19) Bataille, T.; Auffrédic, J.-P.; Louër, D. *Chem. Mater.* **1999**, *11*, 1559−1567.

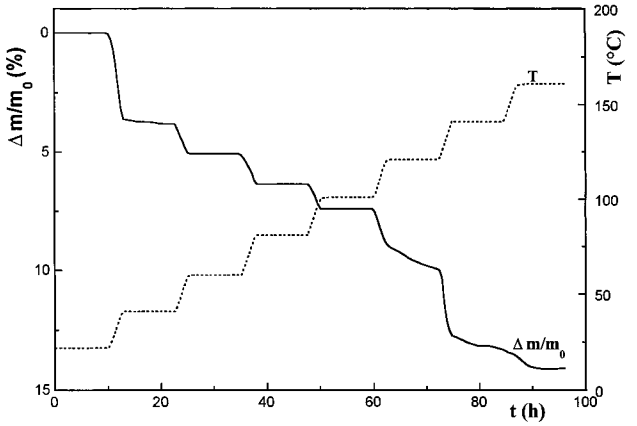

Figure 8. TG curve for the dehydration of $Pb_2Zr(C_2O_4)_4 \cdot nH_2O$ under a water vapor pressure of 6 Torr ($n = 7.75$), showing that the water content is constant at a given temperature.

As already discussed, atoms Ow1 and Ow2 have high atomic displacement parameters (see Table 2), which suggests that these water molecules can leave the structure during the dehydration process. The subsequent effect should clearly be a decrease of coordination numbers of Pb1 and Pb2 from 9 and 8 to 8 and 6, respectively. Such a suggested mechanism is consistent with the high flexibility of lead coordination polyhedra, which are often far from regular and present various coordination numbers.[20] With this interpretation the limit case would correspond to a compound containing two water molecules. This is consistent with the results in Figure 6 showing that still for $n = 3$ the crystallinity of the compound is visible, while for $n = 1.1$ the material is amorphous to X-rays. It has to be noted that the cell parameters reported from the structure determination [$a = 9.537(1)$ Å, $b = 29.622(3)$ Å, $c = 8.9398(9)$ Å, $\beta = 121.19(4)°$, $V = 2160.5(3)$ Å^3] were obtained from a sample in ambient conditions at 22 °C. From Figure 7, it can be seen that the water content in the sample should be, to within experimental errors, approximately 8 instead of 6 as found from the structure analysis. To explain this discrepancy it must be concluded that unidentified diffuse zeolitic water molecules are probably present within the framework of the structure. Nevertheless, attempts to locate them from the powder diffraction data were unsuccessful.

4. Thermal Behavior

4.1. Dehydration. To describe thoroughly the dynamic dehydration process of $Pb_2Zr(C_2O_4)_4 \cdot nH_2O$ experiments were performed under selected water vapor pressures. Figure 8 displays the TG curve recorded under $P'(H_2O) = 6$ Torr ($n = 7.75$), with temperature stages scanned every 20 °C over the range 21−160 °C. It shows that a plateau is obtained for each selected temperature stage up to about 100 °C, for which the water content inside the phase is close to 3.7. In addition, the rehydration process occurs immediately upon cooling. On the other hand, at each temperature stage beyond 100 °C the sample dehydrates continuously. At 160 °C a plateau is obtained ($\Delta m/m_0 = 14\%$).

(20) Steele, I. M.; Pluth, J. J.; Richardson, J. W. *J. Solid State Chem.* **1997**, *132*, 173−181.

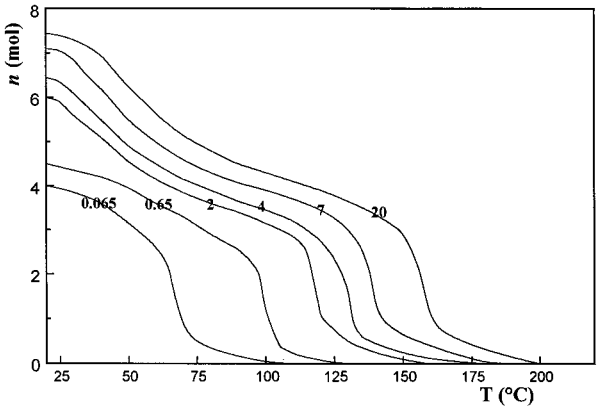

Figure 9. Water content n as a function of temperature for various water vapor pressures $P(H_2O)$ in the range 0.065−20 Torr.

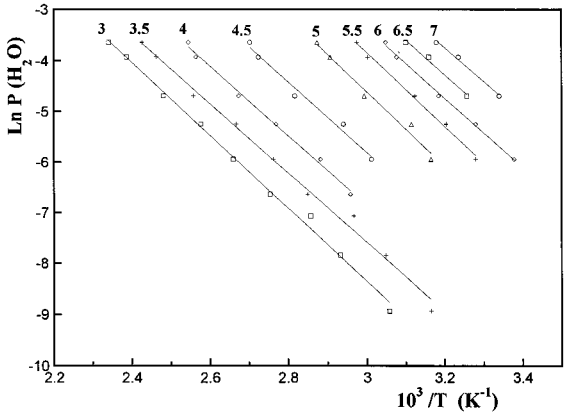

Figure 10. Plot of ln $P(H_2O)$ versus T^{-1} for various water contents in $Pb_2Zr(C_2O_4)_4 \cdot nH_2O$ ($3 < n < 7$).

It corresponds to the formation of the anhydrous phase $Pb_2Zr(C_2O_4)_4$, which is amorphous to X-rays as shown in Figure 6 and is stable until ∼240 °C. Similar results were obtained for other pressures $P'(H_2O)$. These features demonstrate that the number of water molecules exceeding ∼3.5 depends on both the water vapor pressure and the temperature; i.e., the system is divariant. Consequently, these water molecules inside the structure framework can be considered as zeolitic water. Similar results were obtained when the material was submitted to a total pressure $P(H_2O)$. Figure 9 shows representative curves $n-T$ obtained for selected pressures $P(H_2O)$. From these plots, it is easy to determine the equilibrium parameters $P(H_2O)-T$ for a given value n. From Figure 10 it can be seen that $P(H_2O)$ fits the general relationship for n values ranged from 3 to 7

$$\ln P(H_2O) = (A/T) + B$$

The enthalpy change $\Delta_r H$ and the entropy change $\Delta_r S$ for the departure of one water molecule from the precursor containing n water molecules ($3 \le n \le 7$) were calculated from the slope A and the intercept B, respectively. The corresponding values are summarized in Table 4. $\Delta_r H$ is independent of n, and the mean value 58.6 kJ mol^{-1} is slightly greater than the mean value 55.2 kJ mol^{-1} observed for a large number of hydrated salts.[21] On the contrary, $\Delta_r S$ decreases from about 146 to 110 J mol^{-1} K^{-1} when n varies from 5 to 3.

Table 4. Dependence of the Enthalpy $\Delta_r H$ and the Entropy $\Delta_r S$ of Dehydration of $Pb_2Zr(C_2O_4)_4 \cdot nH_2O$ with the Number *n* of Water Molecules in the Material

n	$\Delta_r H$ (J mol^{-1})	$\Delta_r S$ (J mol^{-1} K^{-1})	*n*	$\Delta_r H$ (J mol^{-1})	$\Delta_r S$ (J mol^{-1} K^{-1})
7	55 180	146	4.5	57 750	126
6.5	56 640	146	4	57 000	114
6	56 840	143	3.5	56 840	107
5.5	60 500	150	3	59 800	110
5	61 160	145			

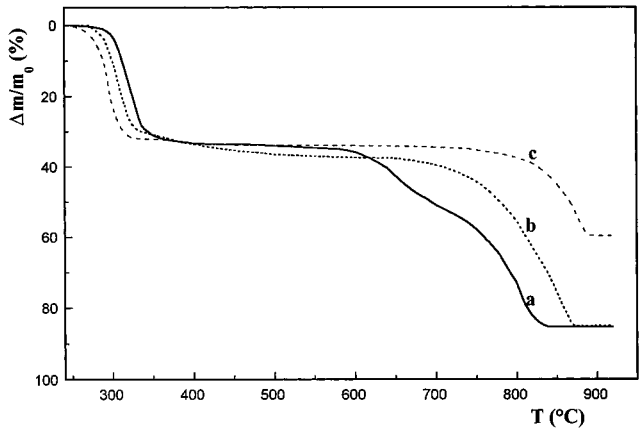

Figure 11. TG curve of the decomposition of $Pb_2Zr(C_2O_4)_4$ under (a) vacuum, (b) $P(H_2O) = 10$ Torr, and (c) nitrogen (sample mass ~50 mg, heating rate 20 °C h^{-1}).

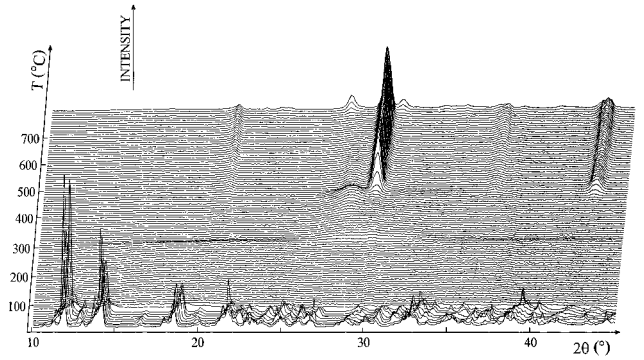

Figure 12. TDXD plot for $Pb_2Zr(C_2O_4)_4 \cdot nH_2O$ under vacuum (heating rate 13 °C h^{-1}; counting time, 2200 s per pattern).

4.2. Decomposition of the Anhydrous Oxalate. Figure 11 gives the TG curves recorded during the decomposition of $Pb_2Zr(C_2O_4)_4$ at a heating rate of 20 °C h^{-1} under vacuum (curve a), under $P(H_2O) = 10$ Torr (curve b), and under nitrogen (curve c). Depending on the atmosphere, weight losses occur from about 250 °C and reach values in the range 33.5−35.5% at 450 °C, which correspond either to the formation of the mixture of PbO and $PbZrO_3$ (theoretical weight loss 33.58%) or to that of the mixture of Pb and $PbZrO_3$ (theoretical weight loss 35.44%). The corresponding TDXD plots under vacuum and under nitrogen are shown in Figures 12 and 13, respectively. In the initial stages of the plots the apparent scrambling of the patterns is due to the changes of the cell parameters with the water content, as already described (see Figure 7). After a temperature range corresponding to a phase amorphous to X-rays,

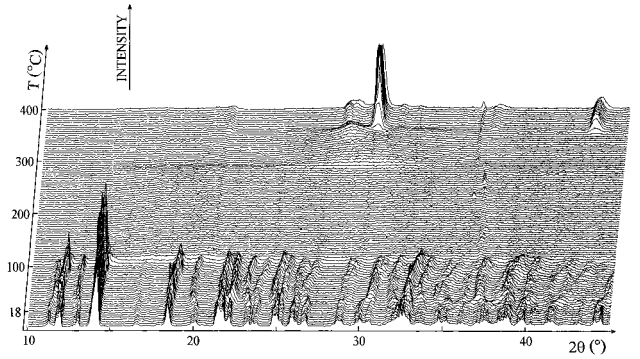

Figure 13. TDXD plot for $Pb_2Zr(C_2O_4)_4 \cdot nH_2O$ under nitrogen (heating rate, 6 °C h^{-1}; counting time, 2700 s per pattern).

the TDXD plots clearly show the emergence of a broad diffraction line with low intensity in the angular range 27−31° (2θ) from about 300 °C. The breadth of this line decreases upon heating until 350 °C under nitrogen or 460 °C under vacuum, where a fast crystallization of $PbZrO_3$ takes place. To elucidate the nature of the compound from which arises this diffraction line a sample heated under vacuum until 420 °C with a heating rate of 10 °C h^{-1} was cooled at room temperature and then analyzed from X-ray diffraction. Although only broad lines are observed (Figure 14), the interrogation of the ICDD PDF-2 database[16] shows that they correspond to the two varieties of PbO, i.e., litharge and massicot. Similar results were obtained under nitrogen, using the same heating rate. Then, it can be suggested that the amorphous anhydrous oxalate gives first a mixture of poorly crystalline PbO and amorphous $PbZrO_3$. Subsequently on further heating crystalline PbO and $PbZrO_3$ are obtained.

To understand the slight differences between the weight losses observed on the TG curves, which seem to depend on the atmosphere, complementary decomposition runs were performed up to 420 °C under the three atmospheres with heating rates in the range 10−400 °C h^{-1} and the final products, cooled at room temperature, were analyzed by X-ray powder diffraction. Figure 14 displays the diffraction patterns for samples obtained under vacuum at three heating rates. The results of these analyses are summarized in Table 5. It can be seen that the nature of the crystalline phases obtained at 420 °C depends on both the atmosphere and the heating rate. The diffraction pattern of the sample prepared with the higher heating rate (400 °C h^{-1}) shows the formation of metallic lead together with an "additional phase" characterized by a very broad line [fwhm = 3.50° (2θ)] at 29.54° (2θ). According to Wilkinson et al.,[22] who studied the crystallization process of PZ from an alkoxide gel with a fast heating rate (600 °C h^{-1}), this line could be assigned to fluorite solid-solution type material. On the other hand, lead was always observed under water vapor pressure.

The formation of lead instead of lead oxide as a decomposition product of anhydrous oxalate is a bit surprising since liquid lead has a high affinity for oxygen at elevated temperature. Indeed, the oxygen vapor pressure in equilibrium with liquid lead and solid

(21) Grindstaff, W. K.; Fogel, N. *J. Chem. Soc., Dalton Trans.* **1972**, 1476−1481.

(22) Wilkinson, A. P.; Speck J. S.; Cheetham, A. K.; Natarajan, S.; Thomas, J. M. *Chem. Mater.* **1994**, *6*, 750−754.

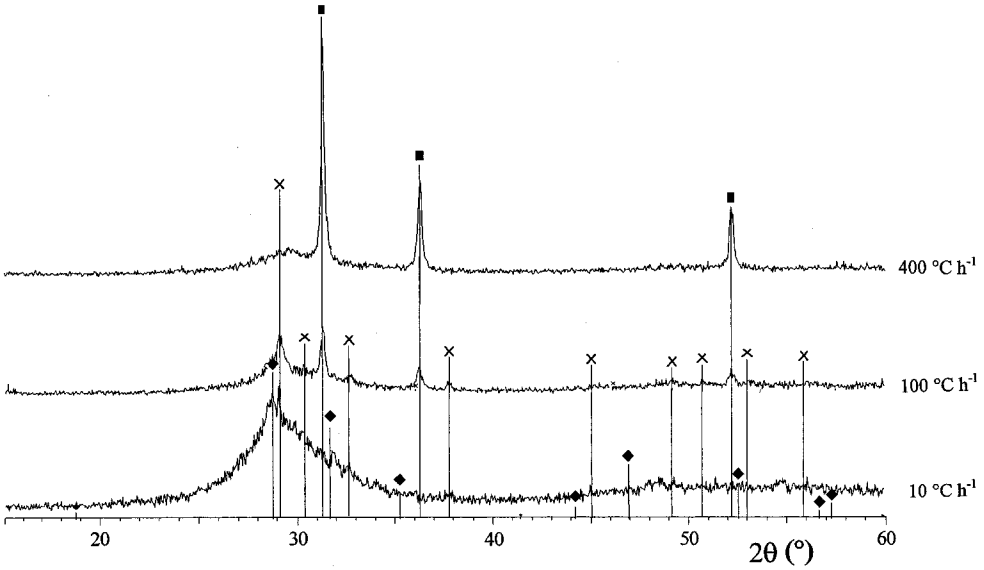

Figure 14. X-ray powder diffraction patterns of the decomposition products obtained at 420 °C at three heating rates and cooled at room temperature: ♦, PbO litharge; ×, PbO massicot; ■, Pb.

Table 5. Phases Identified from the Decomposition of $Pb_2Zr(C_2O_4)_4$ at 420 °C as a Function of the Atmosphere and Heating Rate (after Cooling at Room Temperature)

atmosphere	heating rate (°C h^{-1})	sample color	phases
vacuum	10	yellow	PbO[a]
	50	yellow	PbO[a]
	125	black + yellow	Pb + PbO[a]
	240	black	Pb
	400	black	Pb + additional phase
nitrogen	10[b]	yellow	PbO[a]
	100	black + yellow	Pb + PbO[a]
	400	black	Pb + additional phase
$P(H_2O) = 10$ Torr	10	black	Pb + additional phase
	400	black	Pb + additional phase

[a] Mixture of the two varieties of PbO, litharge and massicot. [b] Until 350 °C only.

lead oxide is calculated to be only 5.25×10^{-17} Pa at 700 K from thermodynamic tables.[23] Under primary vacuum or in pure nitrogen atmosphere oxygen pressures can be estimated to ~0.25 and ~1 Pa, respectively, which are much greater than the equilibrium pressure, and then metallic lead should not be expected. However, it is well-known that the rate of the oxidation process of liquid lead is low.[24,25] This feature is well pointed out in this study since the amount of PbO increases with a lowering of the heating rate. On the other hand, the presence of water vapor pressure decreases the oxidation rate since metallic lead is the alone phase obtained in this atmosphere. The formation of metallic lead has already been reported, e.g., during the decomposition under vacuum or nitrogen of lead titanyl oxalate, when it is carried out with a high heating rate.[26] Finally, it can be stated that the decomposition of $Pb_2Zr(C_2O_4)_4$ carried out at low heating rate leads first to a mixture of lead zirconate PZ and metallic lead, which subsequently can give PbO from a slow oxidation process. On further heating, either liquid lead is vaporized or lead oxide is sublimated, and both were found deposited on the cooler parts of the reaction vessel. Moreover, as already reported, PZ decomposes to form ZrO_2 and again PbO, which is immediately sublimated.[27] These features are well demonstrated in the TDXD plot (Figure 12) which shows that the diffraction lines of PbO disappear above 600 °C, while those of ZrO_2 emerge from ~770 °C. From all the results described in this section the main reaction of the decomposition of $Pb_2Zr(C_2O_4)_4$ performed at low heating rate is

$$Pb_2Zr(C_2O_4)_4(s) \rightarrow Pb(s) + PbZrO_3(s) + 3CO(g) + 5CO_2(g)$$

followed by subsequent reactions giving pure PZ or ZrO_2.

5. Concluding Remarks

The present study demonstrates the existence of a mixed lead zirconium oxalate containing a varying number of water molecules, in the approximate range 3−9, with zeolitic properties. The impact of modern powder crystallography in the field of solid-state chemistry[6] is again highlighted by the determination ab initio of the complex crystal structure of $Pb_2Zr(C_2O_4)_4 \cdot 6H_2O$.

(23) Stull, D. R.; Prophet, H. *JANAF Thermochemical Tables*, 2nd ed.; NSRDS-NBS 37; National Bureau of Standards (U.S.): Washington, DC, 1971.
(24) Azzopardi, M.; Galerie, A.; Besson, J. *Bull. Soc. Chim. Fr.* **1972**, *10*, 3684−3686.
(25) Hope, G. A. *Aust. J. Chem.* **1980**, *33*, 471−480.
(26) Gopalakrishna Murthy, H. S.; Subba Rao, M.; Narayanan Kutty, T. R. *J. Inorg. Nucl. Chem.* **1976**, *38*, 417−419.
(27) Northrop, D. A. *J. Am. Ceram. Soc.* **1968**, *51*, 357−361.

Even though the atomic displacement parameters of the light oxygen atoms are generally not reliable for this kind of materials, the high magnitude of some of them has however been used to suggest a scheme for the release of some water molecules during dehydration. This approach has been found consistent with the high flexibility and coordination changes of lead. The dynamic properties of the water molecules have been carefully confirmed from the calculation of thermodynamical (enthalpy and entropy) data. It should also be noted that, as already reported for oxalate materials,[19] the water molecule content of the partially hydrated phases is correlated to the unit cell parameters. As expected in the Introduction, a mixed PZ oxide is formed during the thermal decomposition according to a complex mechanism depending on the reactional atmosphere. Nevertheless, PZ is often mixed to metallic lead or lead oxide. Pure PZ is only obtained at high temperature, under nitrogen, after vaporization of lead or sublimation of lead oxides. The precise description of the thermal behavior has also greatly benefited from the temperature-dependent powder diffraction study, which allowed identifying in situ the phases formed during the decomposition under various atmospheres.

CM001063J